Ferroelectrics, 477: 65–76, 2015

ISSN: 0015-0193 print / 1563-5112 online
DOI: 10.1080/00150193.2015.999632

Taylor & Francis
Taylor & Francis Group

Scanning Near-Field Optical Microscopy of Light Emitting Semiconductor Nanostructures

A. V. ANKUDINOV,[1,2,*] A. M. MINTAIROV,[1,3]
S. O. SLIPCHENKO,[1] A. V. SHELAEV,[4] M. L. YANUL,[4]
P. S. DOROZHKIN,[4] AND N. V. VISHNYAKOV[5]

[1]Ioffe Institute, 194021 Saint Petersburg, Russia
[2]University ITMO, 197101 Saint Petersburg, Russia
[3]University Notre Dame, Notre Dame, 46556 IN, USA
[4]NT-MDT Co., Zelenograd, 124482 Moscow, Russia
[5]Ryazan State Radioengineering Academy, 391000 Ryazan, Russia

A technique of cantilever based scanning near-field optical microscopy is applied. Using InP/GaInP quantum dots structures, 100nm (λ/7) spatial resolution of the technique in illumination-collection regime is tested. The possibility to obtain optical data with a subdiffraction resolution is exploited for clarifying the transversal electric field mode configuration of the radiating semiconductor laser.

Keywords SNOM; atomic force microscopy; quantum dots; semiconductor laser; luminescence

1. Introduction

One of the ways [1] to surpass the diffraction limit in optical microscopy is to use a special-purpose device with a nanometer aperture and opening in a nontransparent screen. There exist two commercially available configurations for an implementation of this principle: scanning near-field optical microscopy (SNOM) with a fiber-optic probe [2] and the so-called cantilever SNOM [3]. The main advantage of the second variant is in the possibility of controlling orders of magnitude lower forces of interaction with a sample, compared with the case of a fiber-optic probe.

In our study, the SNOM principle was implemented with a cantilever probe with a subwavelength aperture, through which not only the emission could be collected, but also the sample could be simultaneously illuminated. We examined first a sample of self-organized semiconductor quantum dots (QDs) with high-intensity luminescence and surface concentration of ~10 μm^{-2}. The QDs are used in modern nanophotonics to create quantum emission sources in a wide spectral range from the ultraviolet (200 nm) to the near-IR, which includes the telecommunication range (1.3–1.5 μm) [4]. SNOM measurements,

Received July 15, 2014; in final form September 30, 2014.
*Corresponding author. E-mail: alexander.ankudinov@mail.ioffe.ru
Color versions of one or more of the figures in the article can be found online at www.tandfonline.com/gfer.

important for optimizing the QD technology, are also a convenient method for testing the working efficiency of the subwavelength aperture.

As a second kind of objects, the high-power semiconductor laser diodes with an active region shifted with respect to the waveguide were chosen. Heterostructures with the so-called broadened waveguide are used to manufacture high-power lasers [5–7]. With increasing thickness, not only the zero-order fundamental mode appears in the waveguide, but also additional transverse modes of higher orders. Most of optical applications require that only the fundamental transverse mode should be preserved. A number of practical applications, e.g., mixing of two laser frequencies from different active regions to generate far-IR emission [8, 9] need certain transverse modes of higher order. Transverse modes can be selected, as demonstrated in Refs. [10, 11], by choosing the position of the active region in the waveguide. To analyze the mode composition, it is important to measure the near-field pattern at the emitting face of the laser with a subwavelength resolution. A rather convenient tool in this context may be the SNOM with an aperture cantilever.

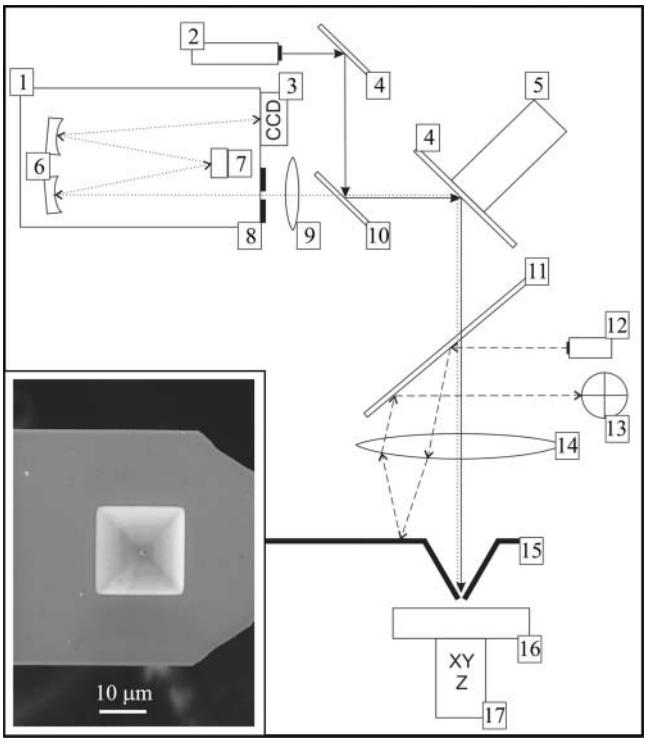

Figure 1. Schematic of the setup: (1) spectrometer, focal distance 520 mm; (2) laser, 473 nm, 50 mW; (3) CCD camera; (4) mirror; (5) tubular piezoscanner; (6) parabolic mirrors; (7) diffraction grating; (8) controllable slit; (9) xyz-adjusted objective lens; (10) edge filter; (11) dichroic mirror; (12) AFM laser, 1064 nm; (13) 4-section photodiode; (14) 100x objective lens; (15) SNOM probe; (16) sample; and (17) piezoscanner. The inset shows a SEM image of the SNOM probe, a cantilever with a subwave aperture at the vertex of the pyramid.

2. Experimental Procedure

The experimental setup, shown schematically in Fig. 1, comprises an atomic-force microscope (NTEGRA Spectra, NT-MDT) and a confocal spectrometer (MS5204i, Sol Instruments). A sample (16) is excited via the subwavelength aperture of a probe (15) by a laser (2) having a wavelength $\lambda = 473$ nm. The laser beam is focused into the region of the aperture by a scanning mirror (4) fixed on a piezoscanner (5) and a large-aperture Mitutoyo objective lens (14) (e.g., 100x with a numerical aperture of 0.7). The emission scattered by the sample is collected by the subwavelength aperture and by the same objective and has two components. The elastically scattered light is reflected from the edge filter (10). The inelastically scattered light passes through the edge filter and is analyzed with a confocal spectrometer (1) with a focal distance of 0.52 m. The spectra are detected with a CCD camera (3), iDus, Andor Co.

Cantilever based probes we used are covered with a nontransparent Al layer on the outer side of a hollow pyramid (inset of Fig. 1). At the tip apex of the pyramid, Al was drilled-off with a focused ion beam to create a through opening (aperture) with a diameter of about 100 nm. The inelastically scattered light that passed through the aperture and collected by the objective lens contains light scattered by the inner surface of the probe and the luminescence signal excited in the sample. In general, the useful contribution of the luminescence is orders of magnitude smaller than the background inelastic scattering from the probe. However, when the probe is brought close to the surface, the background varies under scanning and the total response starts to reflect only changes of the luminescence due to the sample heterogeneities. The background from the probe is further suppressed by using a detection in a confocal mode and a spectral decomposition of the signal using a diffraction grating. The confocal scheme performs a spatial selection by cutting-off the emission from regions far from the aperture. The spectrometer filters out by spectral selection a substantial part of the background from the probe, which lies far from the useful luminescence signal, in the short-wavelength spectral range.

The interaction force between the probe and a sample is controlled by a feedback AFM system. The AFM laser (12) with a wavelength of 1064 nm is focused by the 100x objective lens on the SNOM cantilever (SNOM_NC, NT-MDT). The reflected laser light is collected by the same objective lens and is directed by a dichroic mirror (11) to the four-section photodiode (13).

The SNOM configuration described above makes it possible to measure the luminescence intensity map with a subdiffraction resolution for structures with QDs simultaneously with the topography relief. It is also adapted for a study of light-emitting samples, such as a semiconductor laser diode. In the second case, the high-power laser diode was driven with a pulsed power source to minimize the thermal drift and to stabilize the spectrum and the emission pattern.

3. Results

3.1. Testing the Subwavelength Aperture on a Sample with InP/GaInP QDs

Semiconductor heterostructures with self-organized InP/GaInP QDs were grown on GaAs substrates by metal-organic vapor-phase epitaxy (MOVPE) [12]. The substrate was (100) GaAs misoriented by 2° in the [110] direction having a thickness of 500 μm. First, a 50-nm-thick buffer GaAs layer was deposited, and then a layer of the $Ga_{0.52}In_{0.48}P$ (GaInP) solid solution lattice-matched to GaAs. The QDs were formed at a temperature of 725°C

by deposition of seven monolayers of InP. The growth was completed with deposition of 80-nm-thick GaInP cap layer. It has been shown previously [13] that the QDs have a bimodal size distribution: there are large dots with lateral sizes of 100–200 nm and density of ~$0.5 \times 10^9 \mathrm{cm}^{-2}$ and small dots with lateral sizes of 10–70 nm and density of ~$1.5 \times 10^9\ \mathrm{cm}^{-2}$.

The emission spectrum of the ensemble of QDs, measured in the confocal configuration from an area of several square micrometers, contains two bands peaked at ~740 and ~870 nm (Fig. 2a). To obtain spectra from separate QDs in the near-field configuration, it was necessary to select the aperture cantilevers with improved transmission (~10^{-2}). The transmission of light by the aperture was measured at the excitation wavelength of 473 nm with a detector mounted directly under the probe. Figure 2b shows inelastic scattering spectra for the cases, in which the probe was in static contact with a large QD, or a small QD, or contacted with a surface area free of QDs. The spectra comprise a broad structured band observed at 650-810 nm, associated with the emission from QDs and a band at around 870 nm, related to the GaAs substrate. Only the band peaked at ~740 nm remains in the differential luminescence spectra of QDs (with the subtracted background) (inset in Fig. 2b). It can also be seen that the spectrum is shifted to longer wavelengths with increasing dot size as expected.

Figures 3a–c show a $2 \times 2\ \mu\mathrm{m}^2$ area of AFM surface topography (Fig. 3a) and the luminescence intensity from InP QDs at in the spectral ranges 730–740 nm (Fig. 3b) and 800–810 nm (Fig. 3c). It can be seen that individual QDs are resolved in the luminescence intensity maps. This result demonstrates that such structures are promising for use as test samples for the SNOM technique. There are weak (if any) correlations between

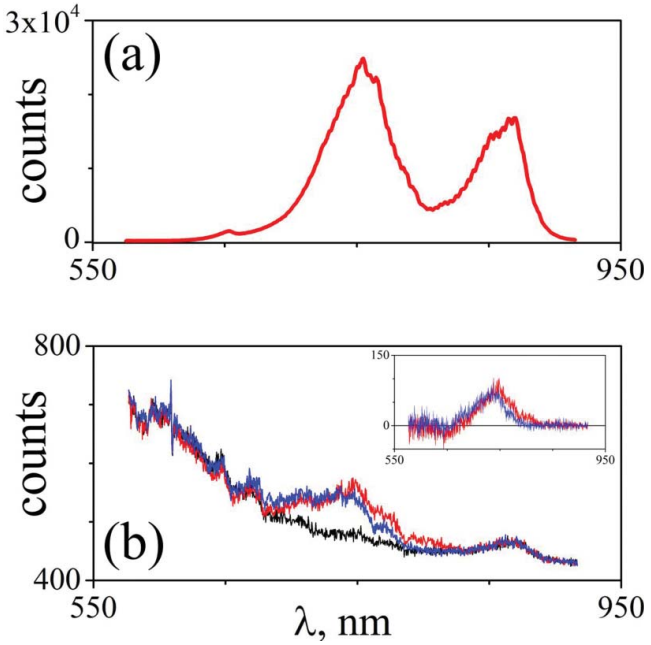

Figure 2. Luminescence spectra of the sample with InP/GaInP QDs measured in (a) confocal and (b) SNOM modes. In (b), the spectrum from the QD-free region (background) is shown by black line; that from a region with a small QD, by blue line; and that from the region with a large QD, by red line. The inset shows spectra from the large and small QD with a subtracted background.

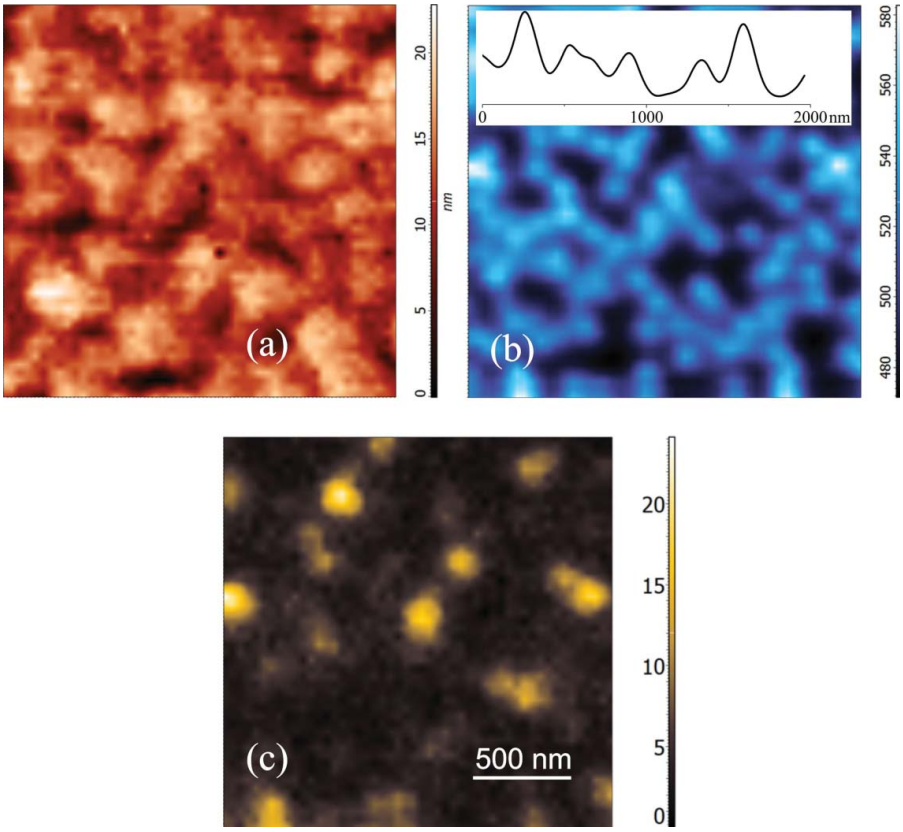

Figure 3. Testing the working capacity of the subwave aperture. (a) Contact AFM image of the surface relief of a 2 × 2 μm^2 part of the sample surface with InP QDs. SNOM maps of the integral luminescence intensity in (b) 730–740 nm and (c) 800–810 nm spectral ranges, measured simultaneously with the AFM image.

the optical and AFM images, which demonstrate that there are no artifacts associated with sample profile height differences in the optical signal. The full width at half-maximum (FWHM) of the optical signal profile taken via individual small QDs is approximately 100 nm (inset in Fig. 3b). Using the Rayleigh criterion and neglecting the real sizes of the 10–70 nm emission source, we obtain a resolution estimate of about 100 nm for the SNOM with the subwavelength aperture used in the study.

3.2. High-Power Semiconductor Laser Diode

3.2.1. Analysis of the Far-Field Emission Divergence. Figure 4 shows the design and characteristics of a high-power semiconductor laser operating at 1.07 μm, based on a heterostructure with wide-bandgap $Al_{0.3}Ga_{0.7}As$ emitters, 1.9-μm-thick GaAs waveguide, and active region with a 8-nm-wide InGaAs quantum well (QW) shifted by 0.75 μm away from the waveguide center toward the p-emitter. A numerical solution of the wave equation for a heterostructure of this kind in the approximation of a dielectric waveguide (with the absorption of light by carriers and the amplification neglected) yields three

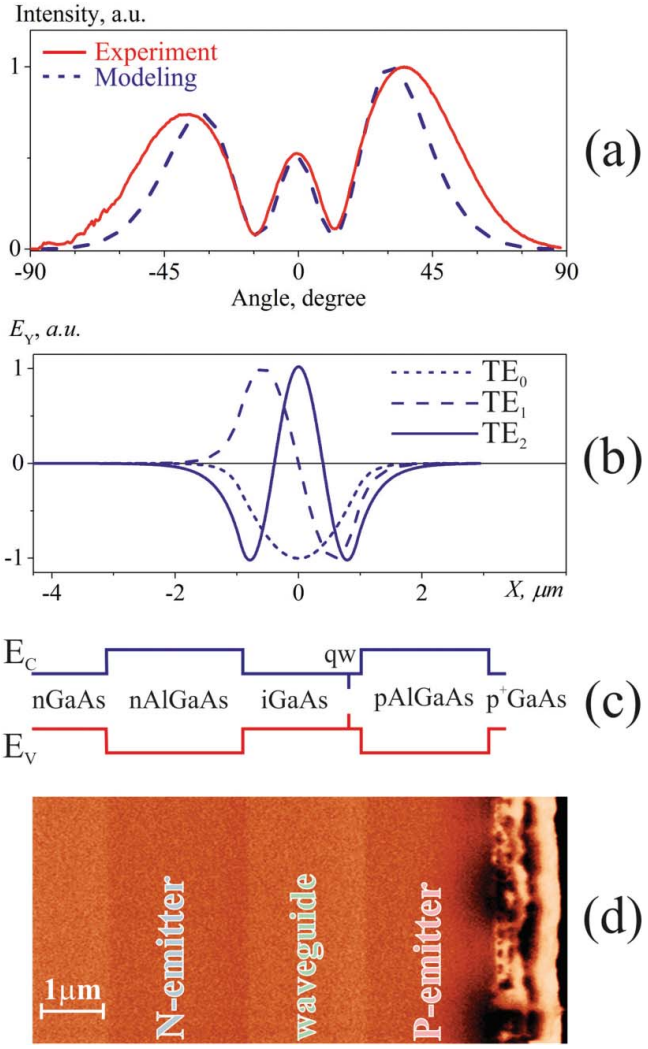

Figure 4. Characteristics and design of a laser diode. (a) Divergence diagram (red solid line) and simulated profile (blue dashed line) calculated for a linear combination of the 2nd and 1st TE modes with an electric field amplitude ratio of 0.267 and a phase difference of 16°. (b) Profiles of TE modes corresponding to the possible solutions to the wave equation for the laser heterostructure. (c) Band diagram of the laser heterostructure. (d) SEM image of the laser mirror surface.

steady-state mode configurations [14]. Figure 4b shows the profiles of all the three TE modes of the electromagnetic field (TE designates the transverse electrical field, whose vector is perpendicular to the emission propagation direction and lies in the QW plane).

It is unlikely that the threshold lasing conditions can be simultaneously satisfied for all three modes. However, analysis of the factors determining the threshold conditions for the 1st and 2nd mode shows the following. The right-hand minimum of the 2nd mode coincides with the QW position (see the band diagram in Fig. 4c), i.e., the QW is effectively overlapped by the electric field. This enables the maximum emission amplification, i.e., creates the most favorable conditions for excitation of the 2nd mode, compared with the other mode structures. It is probable that the 1st mode is simultaneously excited, with

its right-hand minimum also being rather close to the QW. In this case, the lower emission amplification in the active region is compensated by the lower optical loss in the emitter layers. Our calculations demonstrated that, at equal powers of these two modes and medium internal optical loss of 1.5 cm^{-1}, the critical cavity length, at which the threshold lasing conditions are simultaneously satisfied, is 2180 μm. This value is close to the longitudinal size of laser specimens chosen for the experiment.

For the samples under investigation, the experimental far-field radiation pattern in the plane perpendicular to the p-n junction is asymmetric (Fig. 4a). This shape cannot result from an admixture of the even 0th mode to the main 2nd mode, but is due to the simultaneous excitation of the odd 1st mode. The calculated laser emission radiation pattern shown in the same figure is obtained by integration of the near field from a linear combination of the 2nd and 1st TE modes [15, 16]. The calculated and experimental data could be brought to agreement at an approximately fourfold ratio between the electric field amplitudes and a phase difference of 16°. However, other combinations of these modes were also possible, which also satisfactorily describe the experiment. A more accurate and unambiguous information about the configurations of the transverse modes of the laser was obtained in an SNOM analysis of the emission distributions directly at the sites, where the waveguide layers emerge at the surface of the emitting mirror.

3.2.2. Simulation of the Near Field. The two-dimensional wave equation with a single point source at the origin of coordinates has a solution in the form of a zero-order Hankel function, which behaves far from the source as a damped sinusoidal wave $\sin(\omega t - kr)/\sqrt{r}$ [17]. The model brightness signal S(r) is set by a time-average interference intensity I(r,t) of waves of this kind from three sources:

$$
\begin{aligned}
\mathrm{I}(\mathrm{r},\mathrm{t}) &= \left(\frac{\mathrm{A_L}\sin(\omega\mathrm{t}-\mathrm{k}|\mathrm{r}-\mathrm{r_L}|)}{\sqrt{|\mathrm{r}-\mathrm{r_L}|}} + \frac{\mathrm{A_C}\sin(\omega\mathrm{t}-\mathrm{k}|\mathrm{r}-\mathrm{r_C}|)}{\sqrt{|\mathrm{r}-\mathrm{r_C}|}} + \frac{\mathrm{A_R}\sin(\omega\mathrm{t}-\mathrm{k}|\mathrm{r}-\mathrm{r_R}|)}{\sqrt{|\mathrm{r}-\mathrm{r_R}|}} \right)^2, \\
\mathrm{S}(\mathrm{r}) &= \mathrm{I}(\mathrm{r},\mathrm{t}) = \frac{\mathrm{A_L}^2}{2|r-r_\mathrm{L}} + \frac{\mathrm{A_C}^2}{2|r-r_\mathrm{C}} + \frac{\mathrm{A}_R{}^2}{2|r-r_\mathrm{R}} \\
&+ \frac{\mathrm{A_L A_C}\cos(k|r-r_\mathrm{L}|-k|r-r_\mathrm{C}|)}{\sqrt{|\mathrm{r}-\mathrm{r_L}|\cdot|\mathrm{r}-\mathrm{r_c}|}} + \frac{\mathrm{A_L A_R}\cos(\mathrm{k}|\mathrm{r}-\mathrm{r_L}|-\mathrm{k}|\mathrm{r}-\mathrm{r_R}|)}{\sqrt{|\mathrm{r}-\mathrm{r_L}|\cdot|\mathrm{r}-\mathrm{r_R}|}} \\
&+ \frac{\mathrm{A_C A_R}\cos(\mathrm{k}|\mathrm{r}-\mathrm{r_C}|-\mathrm{k}|\mathrm{r}-\mathrm{r_R}|)}{\sqrt{|\mathrm{r}-\mathrm{r_C}|\cdot|\mathrm{r}-\mathrm{r_R}|}}
\end{aligned}
\tag{1}
$$

The wave number $\mathrm{k} = 2\pi/1.07\mu\mathrm{m}^{-1}$; central (C, with a coordinate $\mathrm{r_C}$), left-hand (L, at $\mathrm{r_L}$), and right-hand (R, at $\mathrm{r_R}$) sources were situated at a distance of $3\lambda/4$ from each other, in accordance with the spaces between the extrema of the model near-field profile of the 2nd mode in Fig. 4b. The signal of the simulated image of the 2nd mode is calculated with the following source amplitudes: $A_C = 1, A_L = A_R = -1$. Eq. (1) qualitatively simulates the emission distribution near the mirror not only for the 2nd, but also for the 0th ($A_C = -1, A_L = A_R = 0$) and 1st ($A_C = 0, A_L = A_R = -1$) modes and for a linear combination of all the three modes. In the general case, $\mathrm{A_C}$, $\mathrm{A_L}$, and $\mathrm{A_R}$ are complex numbers.

For the sake of simplicity, we used in the simulation only three point sources and we neglected a minor noncoincidence of the extrema in the electric field distributions of the 1st and 2nd modes. This approach, not intended to be highly accurate, makes it possible to analyze qualitatively the light intensity distribution pattern from the laser for all the possible

mode configurations. We note, in particular, that, according to Eq. (1), the brightness signals near the sources ($S_{L,C,R} := S|_{r=r_{L,C,R}+\varepsilon}$, where ε is infinitely small) obey the proportion $S_L : S_C : S_R = |A_L^2| : |A_C^2| : |A_R^2|$. This circumstance can be used in an analysis of the experimental light intensity signal on the surface of the laser mirror (near-field signal).

3.2.3. Analysis of SNOM Data. The SNOM image of the laser emission distribution over the mirror surface (XY plane) and the contact AFM image of the surface relief, presented in Figs. 5c and 5d, were measured simultaneously. The positions of the

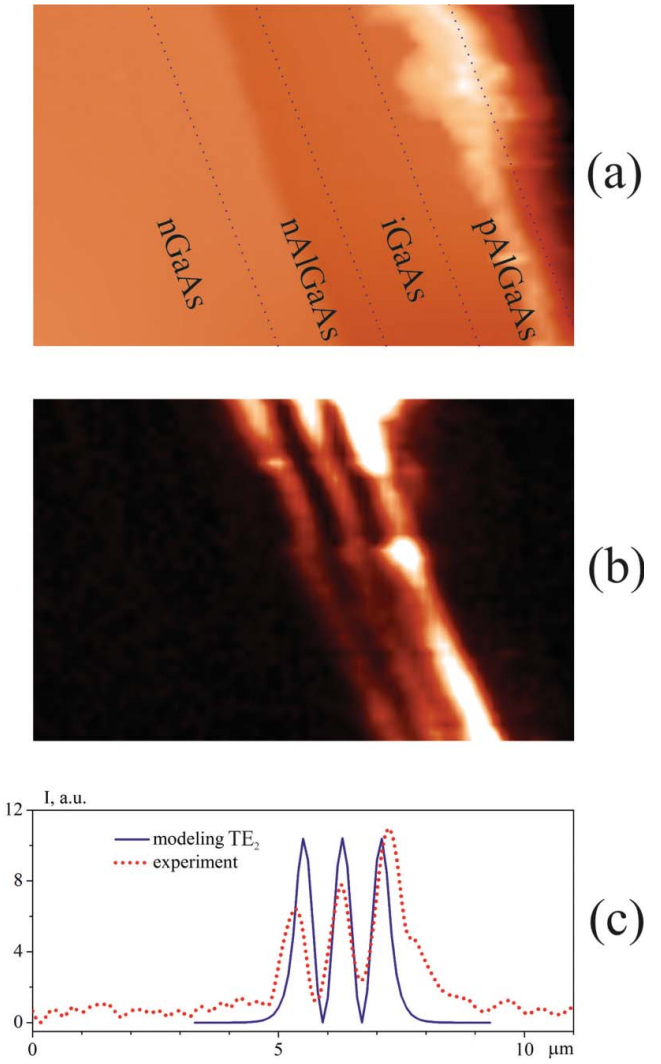

Figure 5. SNOM light-intensity distributions on the mirror of a high-power laser diode operating in the pulsed mode. (a) Contact AFM image of the mirror surface. (b) XY near-field distribution of the laser emission on the mirror. (c) Characteristic near-field profile (red dashed line) and simulated profile (blue solid line) corresponding to the near-field from the 2nd TE mode. Laser feeding and operation parameters: pulse width 5 μs, repetition frequency 1 kHz, amplitude 2A (threshold current 0.35 A), optical power from a single mirror 0.6 W.

main layers of the laser, shown in the AFM image, were reckoned from the cleavage edge by using the known layer thicknesses (Figs. 4c,d). When necessary, measurements revealing all the main layers of the laser heterostructure can be made using a standard cantilever with a sharp probe [18, 19]. According to Fig. 5c, the near-field profile is constituted by three peaks situated in the region, where the waveguide emerges on the surface of the laser mirror. A simulated near-field profile from the 2nd TE mode is superimposed on the figure, together with the characteristic cross-section of the measured signal. In contrast to the simulated distribution, the experimental signal is asymmetric: the right-hand peak is noticeably higher than the left-hand and central peaks.

The observed local near field signal could be formed via admixture of the 1st TE mode (odd mode with two extrema and zero electric field in the middle of the waveguide) to the main 2nd TE mode. A contribution of the 0th mode (single field extremum at the center of the waveguide) to the near field signal is ruled out for two reasons: (i) any linear combination of the 2nd and 0th modes will give a symmetric near field signal and (ii) simultaneous excitation of three modes is unlikely.

In the model with Eq. (1), we can, having measured the peak height ratios in Fig. 5c, $S_L/S_C \cong 0.8, S_R/S_C \cong 1.4$, evaluate the contributions of the 1st and 2nd modes to the near field. We consider the electric field amplitude of the 2nd mode to be unity, and that of the 1st mode, δ; and also set the phase difference φ between the modes. A combination

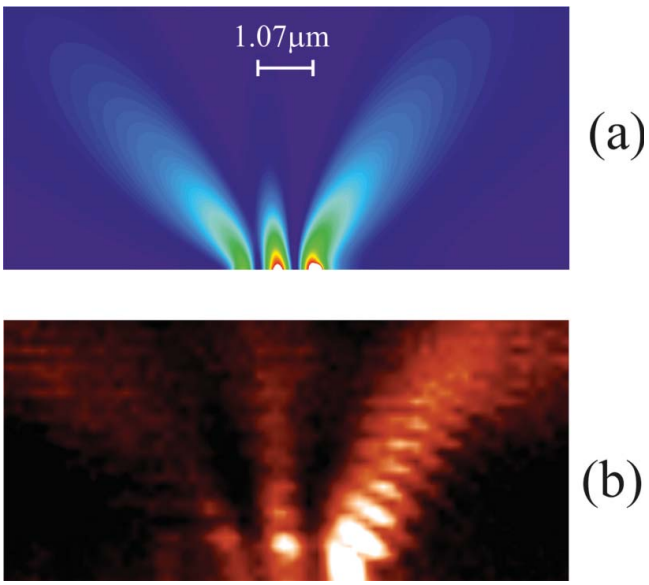

Figure 6. SNOM light-intensity distributions near the mirror of a high-power laser diode operating in the pulsed mode. (a) Simulated XZ image. (b) Experimental XZ distribution of the laser emission signal (integral intensity of the spectrum in the range 1068–1079 nm). The signal of the simulated image was calculated by Eq. (1) with the following values of the parameters: $A_L = -1 + 0.3 \cdot e^{i \cdot \pi/3}; A_C = 1; A_R = -1 - 0.3 \cdot e^{i \cdot \pi/3}$. The simulation also takes into account the deviation of the ridges in Fig. 5b from the scanning axis Y by the angle $\alpha \cong 23^{\circ}$ (distance between the measurement point and the source: $|\mathrm{r} - \mathrm{r_i}| = \sqrt[2]{(\mathrm{z} - \mathrm{z_i})^2 + (\cos\alpha)^2 \times (\mathrm{x} - \mathrm{x_i})^2}; \mathrm{i} = \mathrm{L}, \mathrm{C}, \mathrm{R}$).

of these modes is set by the following values of amplitudes:

$$A_L = -1 + \delta \cdot e^{i\varphi}; A_C = 1; A_R = -1 - \delta \cdot e^{i\varphi} \quad (2)$$

Accounting for $S_L : S_C : S_R = |A_L^2| : |A_C^2| : |A_R^2|$, we can uniquely express the unknown variables in Eq. (2) in terms of the measurable ratios of near-field peaks: $\delta = \sqrt{0.5(S_L/S_C + S_R/S_C - 1}; \cos(\varphi) = (S_R/S_C - S_L/S_C)/(4\delta)$. In particular, we obtain $\delta \cong 0.3, \varphi \cong 60^\circ$ for the data in Figs. 5c and 5d. Thus, the near field locally contains in the measurement region approximately 75% of 2nd mode and 25% of 1st mode. It is noteworthy that the obtained relationships between the phases and amplitudes do not differ strongly from the parameters, at which the calculated and measured far-field divergences are brought in agreement in Fig. 4a: $\delta = 0.267, \varphi = 16^\circ$, which can characterize the near field averaged over the whole 100-μm emission region on the laser mirror.

The experimentally determined composition of the local near field was used to simulate the near field in the XZ plane (Fig. 6a). The SNOM image shown in Fig. 6b demonstrates the propagation of light in three directions (lobes). At a distance of several wavelengths from the surface, the right-hand lobe has the highest intensity, and the central lobe is the weakest. This is in good agreement with the far-field divergence diagram in Fig. 4a and with the results of simulation in Fig. 6a. However, the discrepancy between the experiment and simulation is also well noticeable. While moving away from the surface, the measured intensity of light oscillates with a period of about half the wavelength. There are several signal oscillations on the left-hand and central lobes; these oscillations are best manifested on the right-hand lobe. We attribute these signal oscillations to the interference amplification of light in the cavity formed by the emitting mirror and the probe surface above. This effect is similar to that of antireflection coatings in optical instruments.

4. Conclusions

It has been shown that structures with self-organized InP/GaInP QDs can be used to test the efficiency and ultimate capability of the subwavelength aperture. This tested probe makes it possible to improve the reliability and significance of a subsequent SNOM study. In particular, a resolution of 100 nm (~λ/7) for the optical luminescent signal was achieved in our study of QDs with excitation and collection through the aperture.

The results of an experimental SNOM study and a simulation of the emission distribution near the mirror surface of a high-power laser diode are presented. SNOM images yield an accurate near-field pattern on the laser mirror. However, while moving away from the emitting mirror, the laser light distribution is disturbed. Because of the parasitic interference of light between the probe and mirror surfaces, the spatial signal oscillations appeared masking the emission pattern at the transition to the far-field zone. An asymmetric emission distribution was revealed on the laser mirror surface, in the near field, which indicates that the odd 1st mode is admixed to the main 2nd mode. A satisfactory agreement was obtained between the simulated and experimental results, which made possible to determine the quantitative composition of the local near field: the ratio between the electric field amplitudes of the 2nd and 1st modes and the phase difference.

The demonstrated possibility of solving the inverse problem of reconstructing the near field by using SNOM data seems to be important for the technology of high-power semiconductor lasers with controllable mode composition.

Funding

The work was partially supported by Government of Russian Federation (Grant 074-U01). AMM acknowledges support from the Russian Ministry of Science and Education (Contract No. 14.Z50.31.0021).

References

1. B. Hecht, B. Sick, U. P. Wild, V. Deckert, R. Zenobi, O. J. F. Martin, and D. W. Pohl, Scanning near-field optical microscopy with aperture probes: Fundamentals and applications. J. Chem. Phys. **112**, 7761–7774 (2000).
2. T. Saiki, and K. Matsuda, Near-field optical fiber probe optimized for illumination-collection hybrid mode operation. Appl. Phys. Lett. **74**, 2773–2775 (1999).
3. S. Hosaka, Scanning Near-Field Raman Spectroscopic Microscope. In: Chu P. K., ed. Advances in Solid State Circuits Technologies. Shanghai: InTech China; 2010: 431–446.
4. P. Michler, Single semiconductor quantum dots. Berlin: Springer; 2009.
5. P. Crump, G. Blume, K. Paschke, R. Staske, A. Pietrzak, U. Zeimer, S. Einfeldt, A. Ginolas, F. Bugge, K. Häusler, P. Ressel, H. Wenzel, and G. Erbert, 20W continuous wave reliable operation of 980 nm broad-area single emitter diode lasers with an aperture of 96μm. Proc. SPIE. **7198**, 719814 (2009).
6. S. O. Slipchenko, D. A. Vinokurov, N. A. Pikhtin, Z. N. Sokolova, A. L. Stankevich, I. S. Tarasov, and Z. I. Alferov, Ultralow internal optical loss in separate-confinement quantum-well laser heterostructures. Semiconductors. **38**, 1430–1439 (2004).
7. S. O. Slipchenko, N. A. Pikhtin, N. V. Fetisova, M. A. Khomylev, A. A. Marmalyuk, D. B. Nikitin, A. A. Padalitsa, P. V. Bulaev, I. D. Zalevskiĭ, and I. S. Tarasov, Laser diodes ($\lambda = 0.98\mu$m) with a narrow radiation pattern and low internal optical losses. Technical Physics Letters. **29**, 980–983 (2003).
8. V. Y. Aleshkin, A. A. Afonenko, and N. B. Zvonkov, Difference mode generation in injection lasers. Semiconductors. **35**, 1203–1207 (2001).
9. B. N. Zvonkov, A. A. Biryukov, A. V. Ershov, S. M. Nekorkin, V. Y. Aleshkin, V. I. Gavrilenko, A. A. Dubinov, K. V. Maremyanin, S. V. Morozov, A. A. Belyanin, V. V. Kocharovsky, and V. l. V. Kocharovsky, Room-temperature intracavity difference-frequency generation in butt-joint diode lasers. Appl. Phys. Lett. **92**, 21122 (2008).
10. D. A. Vinokurov, A. L. Stankevich, V. V. Shamakhov, V. A. Kapitonov, A. Y. Leshko, A. V. Lyutetskii, D. N. Nikolaev, N. A. Pikhtin, N. A. Rudova, Z. N. Sokolova, S. O. Slipchenko, M. A. Khomylev, and I. S. Tarasov, High-power lasers (l = 940–980nm) based on asymmetric GaInAs/GaInAsP/AlGaAs separate-confinement heterostructure. Semiconductors. **40**, 745–748 (2006).
11. S. O. Slipchenko, D. A. Vinokurov, N. A. Pikhtin, Z. N. Sokolova, A. L. Stankevich, I. S. Tarasov, and Z. I. Alferov, Ultralow internal optical loss in separate-confinement quantum-well laser heterostructures. Semiconductors. **38**, 1430–1439 (2004).
12. Z. Zhang, L. Yang, V. Liu, T. Hong, K. Vahala, and A. Scherer, Visible submicron microdisk lasers. Appl. Phys. Lett. **90**, 111119 (2007).
13. Y. Chu, A. M. Mintairov, Y. He, J. L. Merz, N. A. Kalyuzhnyy, V. M. Lantratov, and S. A. Mintairov, Lasing of whispering-gallery modes in asymmetric waveguide GaInP micro-disks with InP quantum dots. Phys. Lett. A. **373**, 1185–1188 (2009).
14. S. O. Slipchenko, A. D. Bondarev, D. A. Vinokurov, D. N. Nikolaev, N. V. Fetisova, Z. N. Sokolova, N. A. Pikhtin, and I. S. Tarasov, Selection of Modes in Transverse-Mode Waveguides for Semiconductor Lasers Based on Asymmetric Heterostructures. Semiconductors. **43**, 112–116 (2009).
15. S. A. Akhmanov, and S. Y. Nikitin, Physical optics. New York: Oxford University Press; 1997.
16. H. C. J. Casey, and B. M. Panish, Heterostructure lasers. Part A. Fundamental Principles. New York: Academic Press; 1978.

17. M. Abramowitz, and I. A. Stegun, Handbook of Mathematical Functions. New York: Dover; 1964.
18. A. V. Ankudinov, V. P. Evtikhiev, E\Y Kotelnikov, A. N. Titkov, and R. Laiho, Voltage distributions and nonoptical catastrophic mirror degradation in high power InGaAs/AlGaAs/GaAs lasers studied by Kelvin probe force microscopy. J. Appl. Phys. **93**, 432–437 (2003).
19. A. V. Ankudinov, V. P. Evtikhiev, K. S. Ladutenko, M. G. Rastegaeva, A. N. Titkov, and R. Laiho, Kelvin probe force and surface photovoltage microscopy observation of minority holes leaked from active region of working InGaAs/AlGaAs/GaAs laser diode. J. Appl. Phys. **101**, 024504 (2007).